Co-Design of Highly Efficient Power Amplifier and High-Q Output Bandpass Filter

Kenle Chen, *Student Member, IEEE*, Juseop Lee, *Member, IEEE*, William J. Chappell, *Senior Member, IEEE*, and Dimitrios Peroulis, *Member, IEEE*

***Abstract*—This paper reports the first co-design configuration of a power amplifier (PA) in cascade with a high-Q bandpass filter. By matching the filter's input port directly to the transistor's drain node, the conventional output matching network (OMN) of a PA is entirely eliminated. This leads to smaller size/volume, minimized loss, and enhanced overall performance. To enable this co-design method, the matching-filter synthesis theory is proposed and investigated in detail in this paper. Based on this theory, a 3% bandwidth (centered at 3.03 GHz) two-pole filter, implemented using high-Q evanescent-mode cavity resonators, is designed as the PA OMN to provide optimized fundamental and harmonic impedances for a commercial 10-W GaN transistor. Simulation and measured results show that the co-designed PA-filter module yields a desired Chybeshev filter behavior while maintaining excellent PA performance in the passband with 72% efficiency, 10-W output power, >10-dB gain, and 60-dBm output third-order intercept point. This co-designed module experimentally presents a 8% higher overall efficiency compared to a control group developed using a conventional independent PA and filter, which further validates the effectiveness of this method.**

***Index Terms*—Co-design, efficiency, evanescent-mode (EVA) cavity, filter, GaN, matching network, power amplifier (PA), quality factor, resonator, synthesis.**

I. Introduction

HIGH power amplifiers (PAs) are typically followed by post-selection bandpass filters in modern wireless transmitter front-ends. This cascade topology has been extensively utilized with various functionalities, such as transmitting-channel multiplexing [1], [2], harmonic rejection [3], and spectrum regulation [4], [5]. Moreover, the recently developed digital (burst-mode) transmitters require a low-loss bandpass filter at the PA output to reconstruct the amplitude information from pulse-width or delta–sigma modulation while maintaining a high efficiency and linearity [6]–[8].

Manuscript received April 12, 2013; revised September 15, 2013; accepted September 24, 2013. Date of publication October 10, 2013; date of current version November 01, 2013. This work was supported in part by the National Science Foundation (NSF) under the Enhancing Access to the Radio Spectrum program, Contract 1247893. The work of J. Lee was supported by the Basic Science Research Program through the National Research Foundation of Korea (NRF) funded by the Ministry of Education, Science, and Technology (2012R1A1A1004665).

K. Chen, W. J. Chappell, and D. Peroulis are with the School of Electrical and Computer Engineering and the Birck Nanotechnology Center, Purdue University, West Lafayette, IN 47906 USA (e-mail: chen314@purdue.edu).

J. Lee is with the Department of Computer and Communications Engineering, Korean University, 136-701 Seoul, Korea.

Color versions of one or more of the figures in this paper are available online at http://ieeexplore.ieee.org.

Digital Object Identifier 10.1109/TMTT.2013.2284485

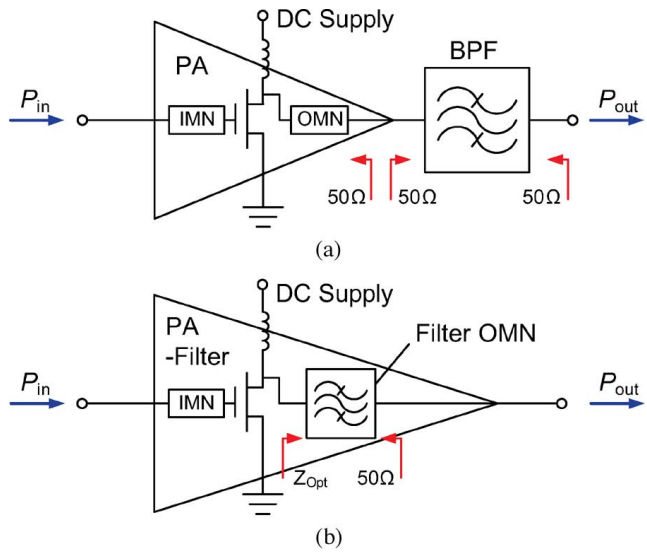

Fig. 1. PA and bandpass filter in cascade. (a) Conventional topology. (b) Co-designed module.

Conventionally, the PA and filter are independently designed based on 50-Ω system impedance, as illustrated in Fig. 1(a). Nevertheless, given the non-negligible insertion loss (IL) of a narrowband filter due to the limited quality factor, the overall performance of a PA-filter module may be degraded significantly, e.g., a 1-dB IL results in a drop of PA efficiency from 80% to ≈60%. Furthermore, additional loss may be introduced from the inter-connection line and mismatch between the PA and filter. To limit the loss term to the lowest possible level, the PA output matching network (OMN) can be entirely eliminated by designing the filter input impedance to directly match the transistor output, which usually needs a non-50-Ω and complex impedance, as shown in Fig. 1(b). This co-design approach leads to a reduced circuit complexity, smaller size/volume, minimized loss, and enhanced overall efficiency. Particularly, it provides an effective solution for the applications in which a small size may take the top priority, e.g., pico and femto base-stations [9], [10].

It is also important to note that in most of the applications, the filter bandwidths need to fit those of the signals [6], [11], which are typically less than 1%. Therefore, resonators with high quality factors are of great importance for such output filters to ensure a low IL and thus a boosted overall system performance. Recently, high-Q ($Q_u > 300$) evanescent-mode (EVA) cavity resonators have been widely exploited to implement narrowband filters [12]–[16], achieving very narrow bandwidths

(<1%), low ILs (<3 dB), and very large spurious-free regions (17:1 in [17]). Compared to the regular rectangular or circular cavities, the EVA cavity yields a good compromise in terms of Q_u and size. Moreover, these EVA cavities can be directly integrated on the same substrate as the PA [13], [15]. Those characteristics particularly enable the co-design technology of the PA and filter.

In [18] and [19], the co-design concept has been investigated with a PA and single resonator. In this research, the co-design approach is expanded to multi-pole filters. As a key enabler for this technology, the matching filter theory is studied in detail in this paper based on the coupling matrix, which is equivalent to the methods presented in [20] and [21]. Specifically, the synthesis of a second-order Chebyshev bandpass filter with non-50-Ω input impedance is presented, which is transformed to a physical design with substrate-integrated EVA cavities. We also present, for the first time, the detailed procedure for realizing the PA-filter module, including filter-response shaping and harmonic matching to perfect the efficiency. The implemented circuit exhibits a desired Chybeshev filter response with an efficient measured performance throughout the passband. Moreover, a standalone PA and filter are developed and cascaded as a control group for performance comparison. It is seen that the overall efficiency of the conventional PA-filter cascade is highly sensitive to the inter-connection-line length. This practical issue can be completely avoided by using the co-design approach, and it experimentally presents an efficiency 8% higher than a specific control group with an inter-connection line of 156° electrical length.

II. Matching Filter Design Theory

Traditionally, microwave circuits are designed under the condition that the impedance of the input and output ports are 50 Ω so that they can be cascaded with other 50-Ω-based microwave circuits. Microwave filters are usually designed such that they exhibit the prescribed frequency response when their input and output ports are connected to 50-Ω systems. Specifically, microwave bandpass filters are initially synthesized with the normalized input and output impedances, while impedance scaling is applied to design 50-Ω-based microwave bandpass filters. However, if another circuit, which is supposed to be connected to the filter, has a non-50-Ω impedance, then a 50-Ω-based microwave filer is not the optimum solution in terms of the maximum power transfer from one circuit to the other circuit in the cascaded system.

In this paper, we design a microwave bandpass filter for connection to the output port of the PA. Conventionally, a PA is realized using a transistor followed by an OMN, which allows us to cascade the PA with other 50-Ω-based microwave circuits. However, this OMN becomes unnecessary if the following stage can provide a desired impedance for the transistor. In the PA-filter case, the microwave filter can be designed to yield a non-50-Ω input impedance desired by the transistor. This co-design method allows us to remove the OMN of the PA.

In this investigation, a second-order Chebyshev-response bandpass filter is designed with 15-dB equi-ripple return loss. A $(N+2)\times(N+2)$ normalized coupling matrix of the second-order filter is given by

$$\mathbf{M}=\begin{bmatrix} 0 & M_{S1} & 0 & 0 \\ M_{S1} & M_{11} & M_{12} & 0 \\ 0 & M_{12} & M_{22} & M_{2L} \\ 0 & 0 & M_{2L} & 0 \end{bmatrix} \tag{1}$$

where M_{S1} and M_{L1} denote input and output external couplings, respectively, and M_{12} represents inter-resonator coupling. M_{11} and M_{22} stand for the detuning of each resonator's resonant frequency from the center frequency of the filter's frequency response. $M_{11}=0$ (or $M_{22}=0$) indicates that the first resonator (or second resonator) is tuned to the center frequency of the filter response. The relationship between a non-zero M_{11} and the resonant frequency of the first resonator (f_1) is given by

$$f_1=f_0\cdot\left[\sqrt{1+\left(\frac{M_{11}\Delta}{2}\right)^2}-\frac{M_{11}\Delta}{2}\right] \tag{2}$$

where f_0 is the center frequency and Δ is the fractional bandwidth. For a non-zero M_{22}, we can find the resonant frequency of the second resonator, f_2, by replacing M_{11} in (1) by M_{22}. The second-order Chebyshev-response bandpass filter with 15-dB equi-ripple return loss for the 1-Ω system can be obtained by using well-known filter synthesis procedures [2], [3], and it is

$$\mathbf{M}=\begin{bmatrix} 0 & 1.037 & 0 & 0 \\ 1.037 & 0 & 1.287 & 0 \\ 0 & 1.287 & 0 & 1.037 \\ 0 & 0 & 1.037 & 0 \end{bmatrix}. \tag{3}$$

The identical response can be obtained for the case that the impedance of the input port of the filter is other than 1-Ω. It can be done by having different M_{S1} and M_{11} values [22]. In this paper, we present a simple design equation so that the filter with an arbitrary input impedance can be designed with ease. It can be derived by considering the normalized input impedance seen looking into the input port of the filter at the center frequency. The filter with the coupling matrix (1) with $M_{22}=0$ has the normalized input impedance of [23]

$$Z_{\text{in}}=\frac{M_{12}^2+jM_{11}M_{2L}^2}{M_{S1}^2M_{2L}^2} \tag{4}$$

at the center frequency. Butterworth and Chebyshev filters have $M_{11}=M_{22}=0$. With $M_{11}=M_{22}=0$, (4) becomes

$$Z_{\text{in}}=\frac{M_{12}^2}{M_{S1}^2M_{2L}^2}. \tag{5}$$

If we want to have the identical frequency response with a different input impedance, the $\mathbf{M}$ values need to be modified. The input impedance of the filter with the coupling matrix

$$\mathbf{M}=\begin{bmatrix} 0 & M'_{S1} & 0 & 0 \\ M'_{S1} & M'_{11} & M_{12} & 0 \\ 0 & M_{12} & M_{22} & M_{2L} \\ 0 & 0 & M_{2L} & 0 \end{bmatrix} \tag{6}$$

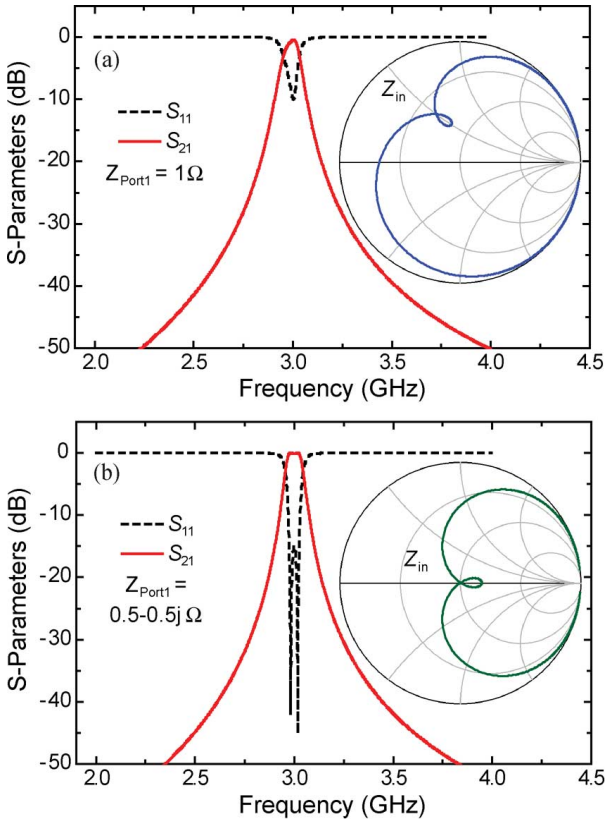

Fig. 2. Frequency responses of the example filter synthesized with non-1-Ω $Z_{\rm in}$: (a) plotted in the regular 1-Ω system and (b) plotted with $Z_{\rm Port1} = 0.5 - 0.5j\ \Omega$.

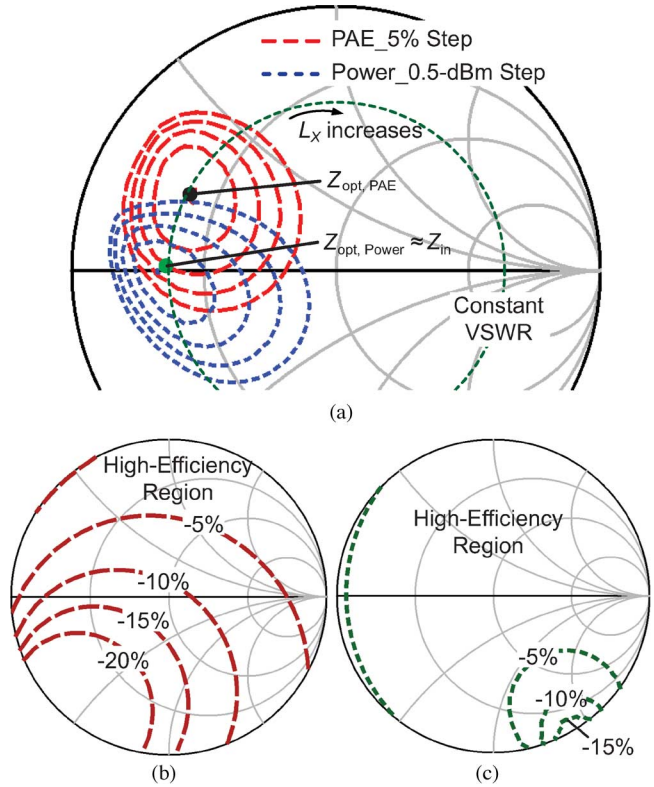

Fig. 3. Load–pull simulation results of the CGH40010 GaN transistor at 3.0 GHz. (a) Fundamental impedance. (b) Second-harmonic impedance. (c) Third-harmonic impedance.

is

$$Z_{\rm in} = x + jy = \frac{M_{12}^2 + jM_{11}'M_{2L}^2}{M_{S1}'^2 M_{2L}^2}. \tag{7}$$

Therefore, the identical frequency response can be achieved when the input port of the filter is connected to a source with the normalized impedance of $x - jy$ under the condition that

$$M_{S1}' = \frac{M_{S1}}{\sqrt{x}}$$
$$M_{11}' = \frac{y}{x} M_{S1}^2. \tag{8}$$

For example, the filter can be designed to have the second-order 15-dB-equiripple Chebyshev response with the normalized input impedance of $0.5 + j0.5\ \Omega$ within the passband by setting $M_{S1}' = 1.467$ and $M_{11}' = 1.075$. Fig. 2 shows the frequency response of the filter designed to have the second-order 15-dB-equiripple Chebyshev response with a normalized input impedance of $0.5 + j0.5\ \Omega$ within the passband, center frequency of 3.0 GHz, and fractional equi-ripple bandwidth of 3%. Fig. 2(a) shows that the filter exhibits a distorted response when its input port is connected to the 1-Ω load. On the other hand, Fig. 2(b) shows that the filter exhibits the desired response when its input port is connected to the $0.5 - 0.5j\ \Omega$ load due to the conjugate matching. It is of note that we can obtain a desired frequency response from a filter with an arbitrary input impedance by synthesizing a filter assuming that the impedance of both input and output ports are 1 Ω followed by modifying M_{S1}' and M_{11}' using (8).

III. Design of High-Q EVA-Cavity Filter as OMN

A. Transistor Selection and Characterization

To experimentally demonstrate the co-design concept of a PA and filter, a GaN transistor (Cree CGH40010F) is selected as the power device of this circuit module. The transistor is characterized using load–pull simulation with Agilent's Advanced Design System (ADS) [24]. The multi-harmonic load–pull simulation results are presented in Fig. 3. Fig. 3(a) shows the optimal fundamental impedances at 3 GHz for achieving maximum power-added efficiency (PAE) and maximum output power, respectively, while the contours of PAE (red in online version) and $P_{\rm out}$ (blue in online version) are also plotted. For PA design at such a high frequency, optimal impedance matching of higher order harmonics is very important to ensure a high PA efficiency. Fig. 3(b) and (c) shows the PAE contours of the second and third harmonics, indicating the regions in which the filter's harmonic impedances need to be located to ensure a high PAE. The load–pull simulation provides the reference impedance for designing the filter as an OMN of the PA.

B. Matching-Filter Realization

Based on the filter synthesis theory presented in Section II, a 3%-bandwidth 15-dB equi-ripple second-order Chebyshev

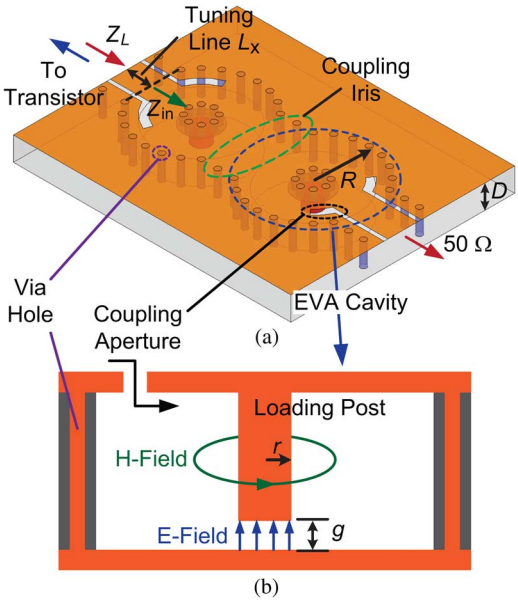

Fig. 4. EVA cavity filter. (a) 3-D illustration. (b) Description of the EVA resonator.

TABLE I
EVA CAVITY PARAMETERS

Parameter	Value
Cavity Radius R	7.2 mm
Cavity Depth D	3.15 mm
Post Radius r	1.2 mm
RF Gap g	20 μm
Simulated Q_u	680
Equivalent Inductance	1.4 nH
Equivalent Capacitance	2.0 pF

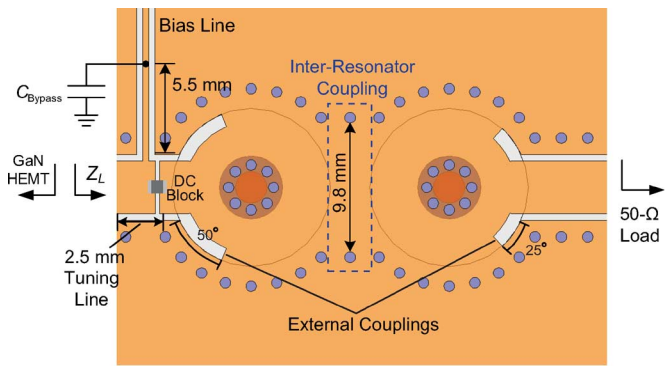

Fig. 5. Finalized OMN with the two-pole EVA cavity filter.

bandpass filter is designed and realized with substrate-integrated EVA cavity resonators, as shown in Fig. 4(a). Fig. 4(b) illustratively shows the cross-section view of a single EVA resonator and the internal electromagnetic field distribution. To implement this resonator in a printed circuit board (PCB) substrate, the electrical boundary of the cavity is defined by via holes, as shown in Fig. 4. By placing a capacitive loading post in the center, the electric field is predominantly concentrated in the gap between the post and the bottom wall, which represents an effective capacitor. The magnetic field circles between the sidewall and the post, forming a shorted coaxial line, which represents an effective inductor. Since the E- and H-field are all stored in air and the current is distributed throughout the side wall, a very high quality factor can be achieved with this resonator type.

The design of an EVA cavity resonator with an optimized quality factor has been well studied in [13], [15], and [16]. This work follows a similar approach in which the modeling and simulation are performed using Ansoft's High Frequency Structure Simulator (HFSS) [25]. The final geometrical dimensions of the EVA cavity is listed in Table I. A gap spacing of 20 μm is selected here to result in a resonant frequency of 3 GHz, and the simulated unloaded quality factor is around 680. The major high-power limitation of the EVA resonator is the gas discharge in the μm-scale gap spacing. It is presented in [26] that the EVA cavities are gas-discharge-free for operating at a 10-W power level, indicating that this design is within the safe range of high-power operation. The two-pole filter is constructed using two EVA resonators, as shown in Fig. 4(a). These two resonators are coupled through a coupling iris that forms the internal coupling coefficient (M_{12}) and determines the filter bandwidth. The external couplings are realized using slot apertures that are aligned with the direction of the magnetic field inside the cavity. The values of the external coupling coefficients, M_{S1} and M_{2L}, are determined by the lengths of the slots. The geometries of these coupling structures are eventually optimized using HFSS, which are indicated in Fig. 5.

In conventional PA design, the impedance of the OMN is normally set to the point that leads to either maximum PAE $(Z_{\mathrm{opt,PAE}})$ or maximum power $(Z_{\mathrm{opt,Power}})$. It can be seen from Fig. 3 that $Z_{\mathrm{opt,PAE}}$ and $Z_{\mathrm{opt,Power}}$ share the same real part ($\approx$11 in this design), while their imaginary parts are both very small ($\mathrm{Im}(Z_{\mathrm{opt,PAE}}) \approx 6\ \Omega$, $\mathrm{Im}(Z_{\mathrm{opt,Power}}) \approx 0\ \Omega$). Therefore, the filter's input impedance Z_{in} is tuned to the real value of 11 Ω by properly selecting M'_{S1} (lengthening the input coupling slot, as shown in Fig. 5) in (7), while the imaginary part of Z_{in} is kept to zero by setting M'_{11} to 0 (resonator 1 is not de-tuned). The small complex offset of Z_{opt} is obtained by placing a short tuning line with length of L_x in front of the filter. It is important to note that this transmission line (TL) is necessary here to place the bias line and dc-block capacitor for the transistor [19]. To match the transistor impedance with a large imaginary part (e.g., a bare-die transistor [27]), a non-zero M'_{11} can be utilized to perform the matching by de-tuning the resonant frequency of resonator 1. This can result in the shortest possible tuning line.

C. Optimization of Fundamental and Harmonic Matchings

The matching filter theory in Section II underlines that a Butterworth or Chebyshev filter response can be achieved for any given impedance of the source. In this co-design case, however, the filter's input port is not matched to a static source impedance, but the transistor's output with a frequency-dependent impedance behavior. Thus, the filter's input impedance needs to be properly selected to result in a desired frequency response of the entire PA-filer module. However, it is found in this design that neither of the conventional optimal points ($Z_{\mathrm{opt,PAE}}$ and $Z_{\mathrm{opt,Power}}$) leads to an expected Chebyshev filter response

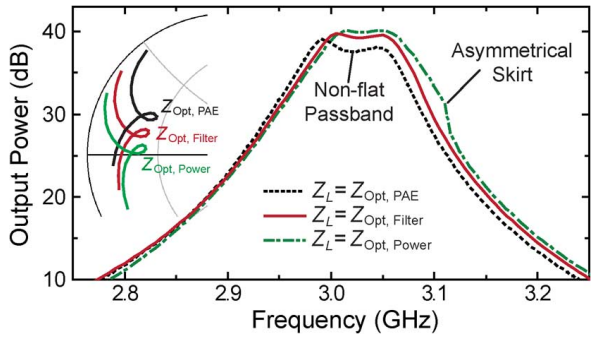

Fig. 6. Simulated output power frequency response under a 28-dBm input stimulus for different load impedance provided by the filter.

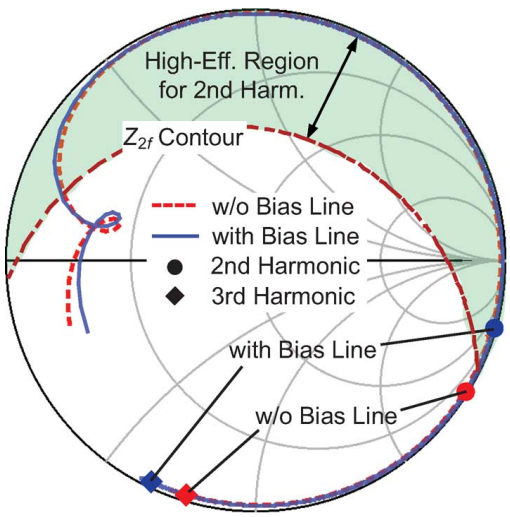

Fig. 7. Simulated Z_L versus frequency provided by the filter.

of the entire module, as indicated in Fig. 6. Using ADS simulation, an optimized filter response (red curve in online version of Fig. 6) can be obtained by optimizing the tuning-line length (L_x). The load impedance Z_L is eventually set to a point in between $Z_{\mathrm{opt,PAE}}$ and $Z_{\mathrm{opt,Power}}$ $(L_x = 2.5$ mm), as shown in the inset of Fig. 6, leading to a flat passband and symmetrical skirt. Fig. 7 shows the input impedance of the designed filter (red dashed line in online version), extracted from full-wave simulation using HFSS. It can be seen that an optimized impedance matching $(Z_L = Z_{\mathrm{opt,Filter}})$ is achieved with this filter, yielding an excellent balance between PA performance and filter shape, which are both important in this co-design case.

In addition to the fundamental impedance matching, harmonic impedance matching is also important for achieving a high efficiency. As shown in Fig. 7, the second harmonic impedance (Z_{2f_0}) of the initial filter does not fall in the high-efficiency region. Therefore, the bias line is utilized to further tune the harmonic impedance, similar to the approach presented in [19]. This bias line is realized using a high-impedance (106 Ω) short-ended TL appended to the TL between transistor and filter. By properly selecting the bias-line length (5.5 mm, ≈30° at 3.1 GHz), the second harmonic impedance is tuned to the high-efficiency region while the fundamental impedance almost remains the same, as shown in Fig. 7. The third harmonic impedance is located in the optimal region for both the initial

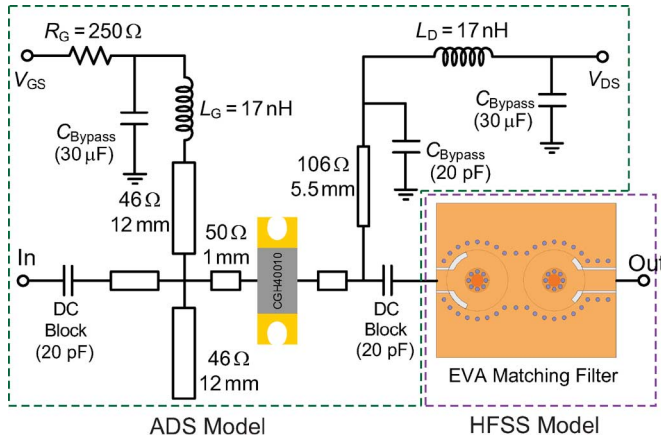

Fig. 8. Circuit schematic of the co-designed PA-filter module.

and bias-line-tuned filters, compared to the load–pull result shown in Fig. 3(c).

IV. Design and Implementation of the Entire PA-Filter Module

A. PA Design

To complete the design of the entire circuit, the input matching network is realized using a single open-ended stub [28], which provides an input impedance of $3-5j\ \Omega$ at 3.0 GHz. The circuit schematic of the co-designed PA-filter module is plotted in Fig. 8. A 17-nH inductor is connected to the end of the stub, and a 250-Ω resistor is in series with the inductor as the amplifier stabilizer. From simulation using manufacturer's models, this network provides an impedance of $|Z| > 350\ \Omega$ at a frequency higher than 3 GHz, which presents an effective open. Another 17-nH inductor is connected to the end of the output bias line to further prevent RF power leakage. This inductor actually has no contribution to the output matching since the bias line is short ended by a bypass capacitor. The two 20-pF capacitors are connected to the transistor's gate and drain as dc-blocks. Those surface mount devices also introduce extra parasitics, which were considered in the circuit design. For example, the parasitics of the output dc-block capacitor, mainly represented by a series inductance, can be compensated by slightly reducing the length of the tuning line [29].

Simulation of the entire circuit schematic is performed using the harmonic-balance (HB) simulator in ADS together with the filter model extracted from HFSS, as described in Fig. 8. Fig. 9(a) shows the simulated efficiency and output power from 2.7 to 3.4 GHz with a constant 28-dBm input stimulus, indicating a 40-dBm output power throughout the passband and a maximum efficiency of 77% at the center frequency of 3.03 GHz. Fig. 9(b) presents the de-embedded drain current and voltage waveforms when the circuit is operating at 3.03 GHz. A high-efficiency operation of the PA can be seen from the current–voltage waveform shape, indicating a harmonic-tuned saturated PA mode [30]–[32].

B. Fabrication

The PA-filter module is fabricated in a single 3.175-mm-thick Rogers TMM3 substrate. The front side and back side of the

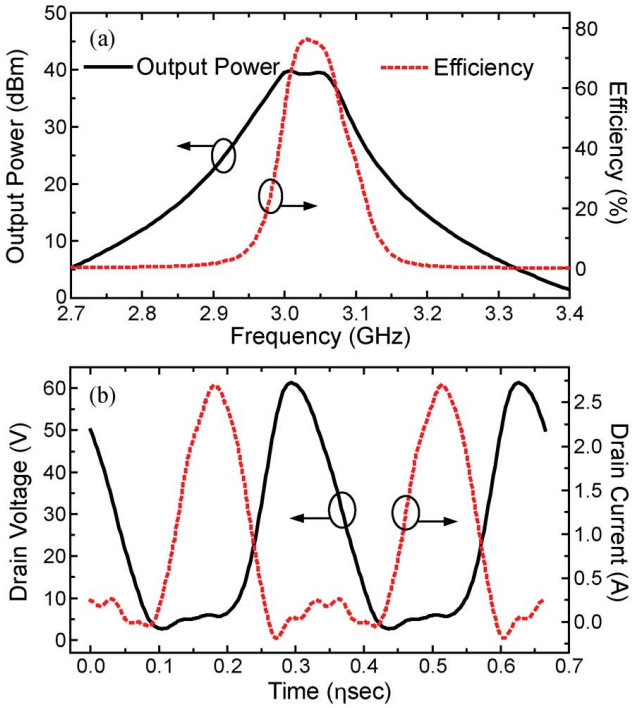

Fig. 9. Simulated results of the circuit schematic. (a) Output power and efficiency versus frequency with a 28-dBm input power. (b) Intrinsic drain waveforms of voltage and current at 3.03 GHz.

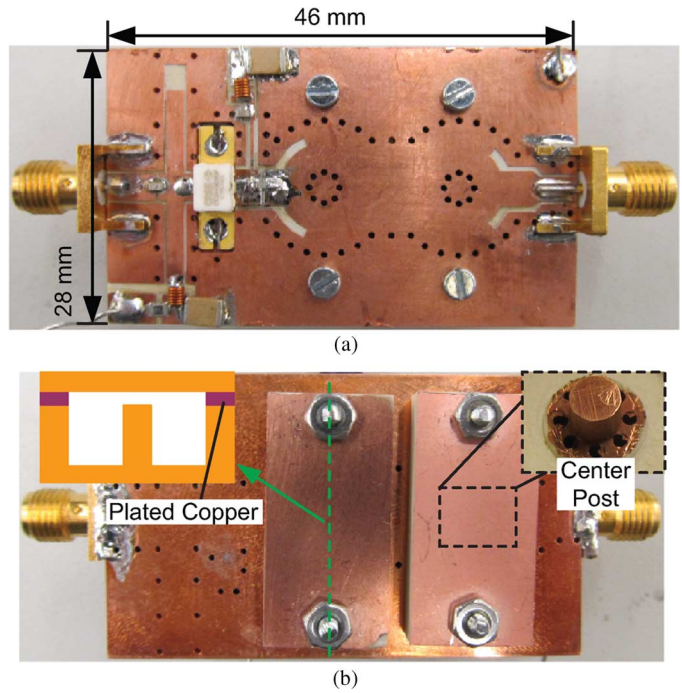

Fig. 10. Fabricated PA-filter co-design module. (a) Front side. (b) Back side.

fabricated circuit are shown in Fig. 10(a) and (b). The packaged transistor is placed in a metallized slot that is cut into the substrate. Fabrication of the EVA cavities follows a process similar to those of the standalone tunable filters in [13] and [16]. The cavity and the capacitive post are milled out inside the substrate. The electrical boundary of the cavity resonator is defined by copper-plated through-substrate vias. To seal the cavity, two thick copper plates are attached to the substrate by mechanical pressure using screws. The desired 20-μm gap is defined by copper plating, as shown in the inset of Fig. 10(b). Compared to our previous works presented in [18] and [19], this fabrication technology avoids the utilization of low-conductivity silver epoxy for cavity sealing, leading to an enhanced quality factor.

V. Experimental Results and Discussions

A. Continuous Wave (CW) Measured Results

The fabricated circuit is first measured using an Agilent E8361C performance network analyzer (PNA). Fig. 11(a) shows the measured small-signal frequency response, including S_{11}, S_{21}, and S_{22}. In this measurement, the transistor gate is biased at a class-AB point, leading to a quiescent current of 260 mA at $V_{\rm DS} = 25$ V. The curves of S_{21} and S_{22} indicate a desired Chebyshev filter shape similar to the standalone filters, while the passband has a small-signal gain of around 15 dB. The simulated equal-ripple return loss (S_{22}) is around 14.5 dB, slightly lower than the design value of 15 dB. This is basically caused by the load-line matching condition imposed in the PA design, introducing slight mismatch in the small-signal case.

The S_{11} shape is similar to a regular PA design, as the high-Q filter is completely isolated by the transistor seen from the input port. The measured reflection coefficient, S_{11}, is from around

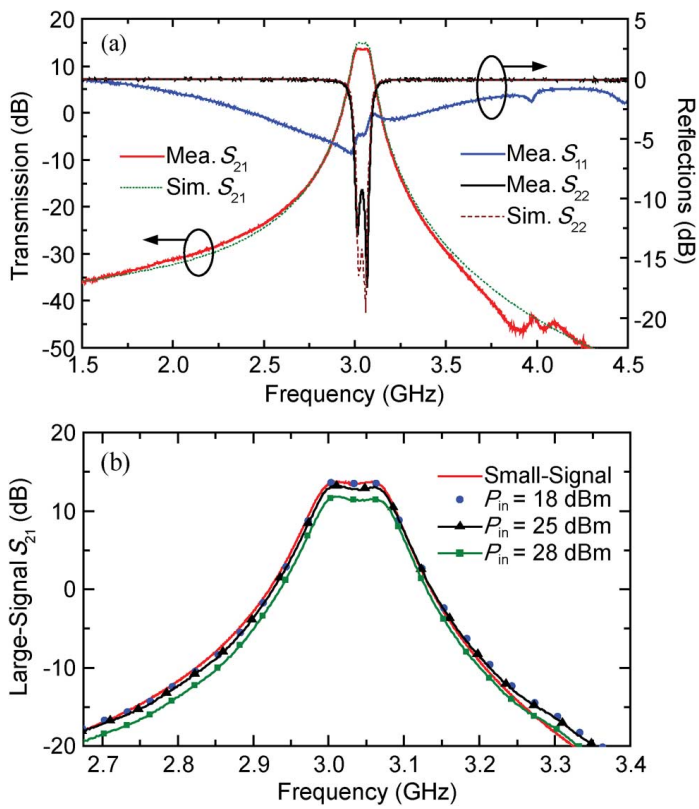

Fig. 11. Measured and simulated frequency responses of the co-designed PA and filter. (a) Small signal. (b) Large signal.

-3 to -7 dB, slightly lower than the regular PA design such as reported in [33]. This is mainly due to the fact that the input matching network in this design does not include any additional stabilization resistance (e.g., series and parallel resistors to the gate) since this amplifier have already been stable. In practical

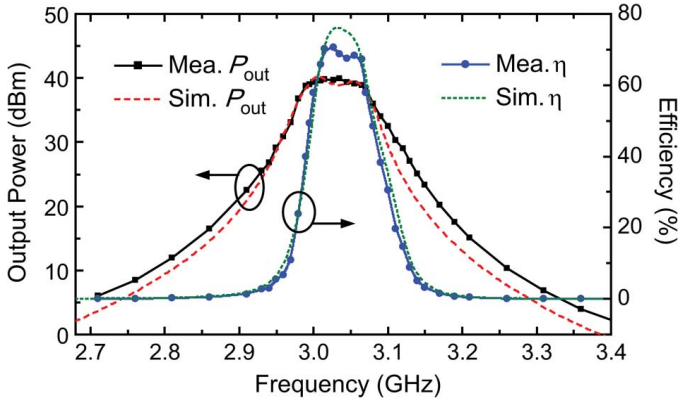

Fig. 12. Measured and simulated PA performance with a 28-dBm frequency-swept input stimulus.

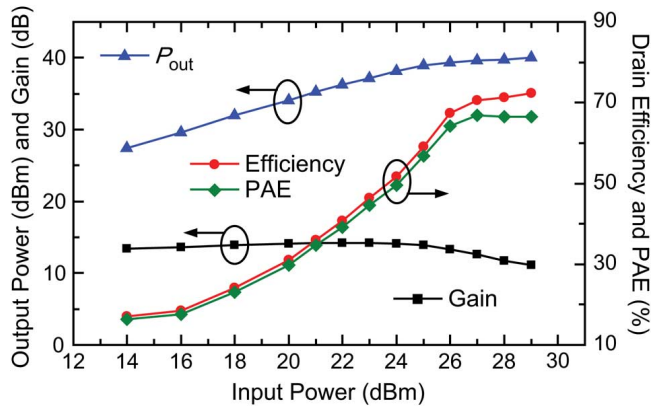

Fig. 13. Measured PA performance versus input power at the center frequency of the passband.

applications, S_{11} might need to be further reduced by improving the input matching [33]. Simulated results are also plotted in Fig. 11(a) for comparison, which match well with the measurement. It is important to highlight that the simulated S_{22} presents a 14.2-dB equi-ripple, slightly lower than the target value of this design. This is mainly due to the slight mismatch in the input port, induced by the load-line matching imposed in the PA design.

Fig. 11(b) shows the large-signal frequency response of the co-design PA-filter circuit. It can be seen that the gain drops as the input power level increases from 18 to 28 dBm, which is due to the PA saturation. At the low input power of 18 dBm, the large-signal frequency response is consistent with the small-signal results, as expected.

The high-power CW test is then performed on the PA-filter module. In this case, the transistor gate is biased at the pinch-off point of 3.3 V, while the drain is maintained at 25 V. The CW signal is generated by an Agilent E4433B signal generator and boosted by a commercial PA (ZHL-16W-43+, Mini-Circuits) to provide a sufficiently large input power to drive this PA-filter module. The PA output power is measured using an Agilent E4419B power meter. Fig. 12 shows the measured output power and efficiency across the frequency range from 2.7 to 3.4 GHz with a constant input power of 28 dBm, indicating a measured efficiency of 71% at the center frequency of 3.05 GHz. An efficiency of $>$50% and output power of 40 dBm were measured across the entire passband. A good agreement between measurement and simulation can also be seen from Fig. 12.

Subsequently, the dynamic response of the PA is measured by varying the input power from 14 to 29 dBm, as shown in Fig. 13. Gain compression occurs when the input power reaches 25 dBm and the highest PAE of 68% is achieved when the input power is greater than 27 dBm. The circuit is further characterized with various drain bias voltages under a constant 28-dBm input stimulus. As shown in Fig. 14, optimized efficiency and PAE are achieved at the drain voltage of 25 V, which is utilized throughout the entire measurement.

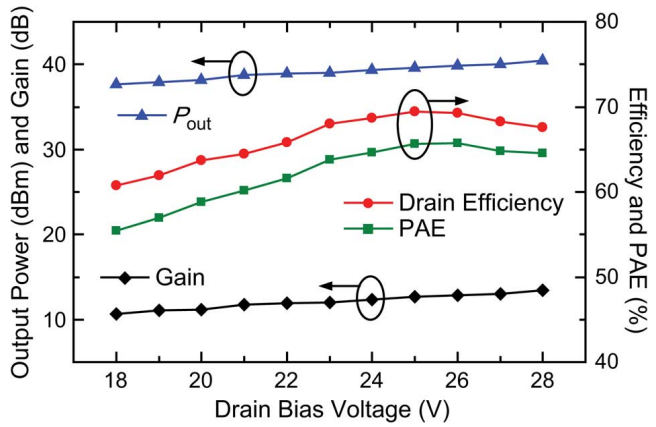

Fig. 14. Measured PA performance under various drain bias conditions.

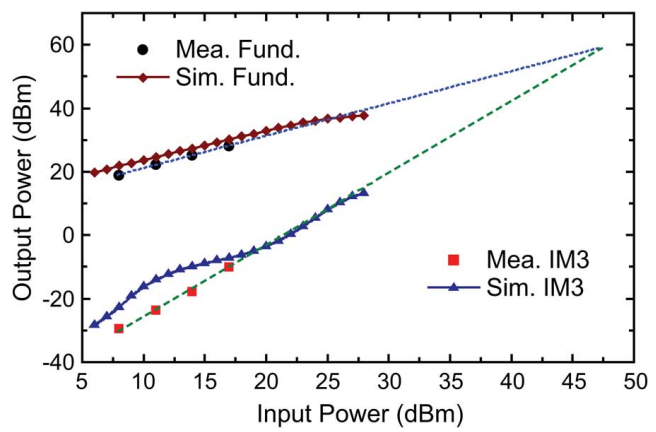

Fig. 15. Measured and simulated linearity performance using two-tone signal.

B. Linearity Evaluation Using Two-Tone Signal

The linearity performance of the co-designed PA and filter is evaluated using a two-tone signal. The two-tone spacing is selected based on the passband of the PA-filter module. Thus, these two tones are placed at the upper and lower edges of the filter passband, i.e., 3 and 3.06 GHz, respectively. Fig. 15 shows the measured and simulated results under a two-tone stimulus, including the output powers of fundamental and third-order intermodulation (IM3) components. The output third-order intercept point (OIP3) is extracted by sweeping the input power of

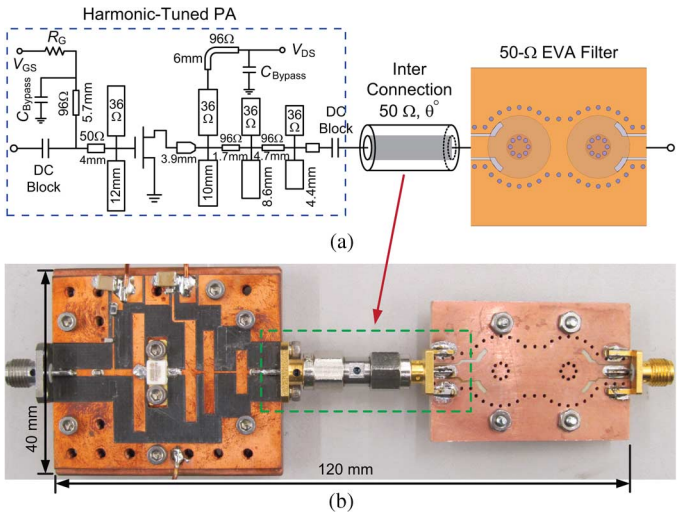

Fig. 16. Independent PA and filter cascade circuit for comparison. (a) Schematic model. (b) Actual circuit.

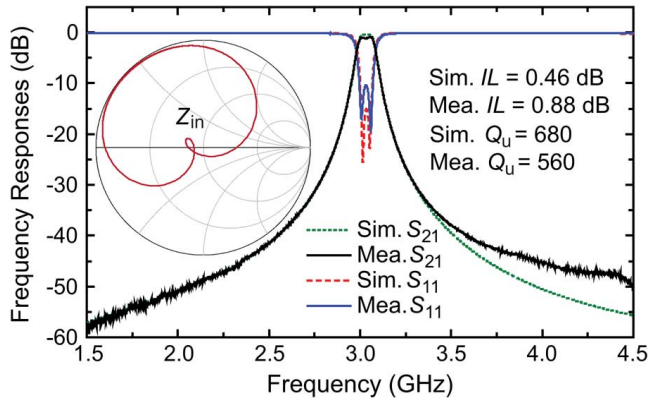

Fig. 17. Measured and simulated frequency response of the 50-Ω filter.

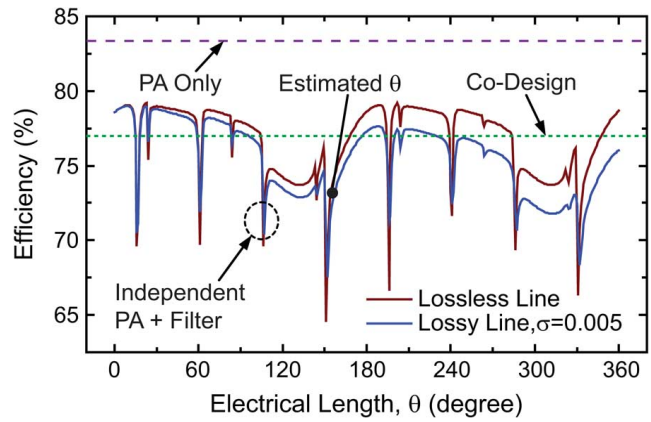

Fig. 18. Simulated effect of inter-connection line (ideal lossless line and lossy line with loss-tangent $\sigma = 0.005$) on the overall performance of the cascade of independent PA and filter.

the two-one signal, as illustrated in Fig. 15, leading to a measured OIP3 of around 60 dBm. It is also seen from the simulation that < -25 dBc of IM3 is achieved even at the saturated power level. These results compare favorably to those of the reported high-linearity PA designs [34], [35], indicating an excellent linearity performance of this PA. This is due to the combined contribution of the PA operation mode and narrowband filtering effect of the OMN.

C. Comparison and Discussions

It has been shown in Sections V-A and V-B that the co-designed PA-filter module exhibits the desired filter behavior in its frequency response and good PA performance in the filter passband. To further validate the effectiveness of this approach compared to the conventional one, a control group is developed with a standalone harmonic-tuned high-efficiency PA and a regular 50-Ω filter, which are connected in cascade via a coaxial adaptor, as shown in Fig. 16. The detailed design of the high-efficiency PA has been presented in [36]. The filter is implemented using the same EVA technology as the one in the co-design module. The simulated and measured frequency responses of the designed filter are shown in Fig. 17, indicating good agreement between these two cases. The simulated and measured ILs are 0.45 and 0.88 dB, respectively. This is mainly due to the slightly degraded Q_u of the fabricated EVA resonator.

For the PA-filter cascade topology in Fig. 16(a), it is found that the overall performance is highly dependent on the electrical length (θ) of the inter-connection structure, which is modeled as a 50-Ω TL in both lossless and lossy cases. This is because the PA is highly sensitive to the output impedance at both fundamental and harmonic frequencies. The reflection between the PA and filter on the inter-connection line is a very complicated phenomenon [37]. However, the overall efficiency of the entire topology can be easily extracted from HB simulation using ADS. It is seen that the filter causes a significant efficiency drop from that of the standalone PA (83.5%) due to the filter's IL and mismatch. The simulated efficiency (at saturated power level) versus θ is plotted in Fig. 18, showing a large fluctuation of the efficiency varying from 65% to 79%. This is mainly due to the fact that the input impedance of the standalone filter is not exactly 50 Ω, as shown in Fig. 17, so that different θ leads to different impedance presented to the PA output. If the loss of the inter-connection line is considered, the efficiency is further degraded as θ increases. The estimated total electrical length of the inter-connection line is around 156°, as indicated in Fig. 18, jointly contributed by the on-board lead TLs and the coaxial adaptor. This leads to an overall efficiency of around 71%–72% for the control group, which is 5% below the co-design case in ADS simulation.

In the experiment, a power-swept CW measurement is conducted with the control group at the center frequency of the filter at around 3.03 GHz. The measured results are shown in Fig. 19 for comparison. It can be seen that the filter experimentally causes an efficiency drop of the PA from 80% to 64% at power saturation of around 40 dBm, while the co-design approach enhances the overall efficiency to around 72%. These results underline that, in a real system, the length of the inter-connection line between the PA and filter needs to be properly tuned to yield a good overall performance, or the filter effect can be lifted by placing a circulator between them. However, both of them lead to increased complexity, space, and loss. The co-design approach is an effective solution that achieves an optimized

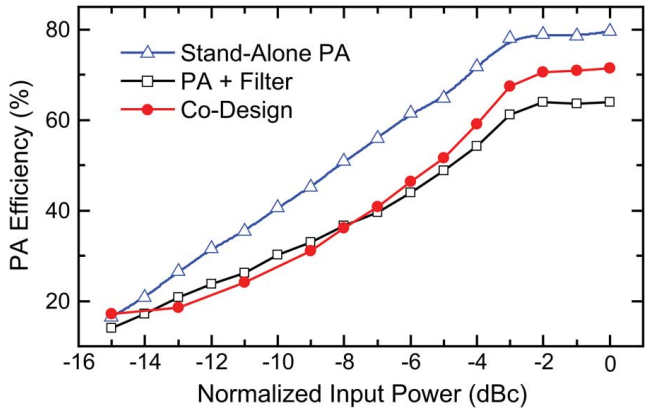

Fig. 19. Comparison of measured performance between conventional and co-designed modules.

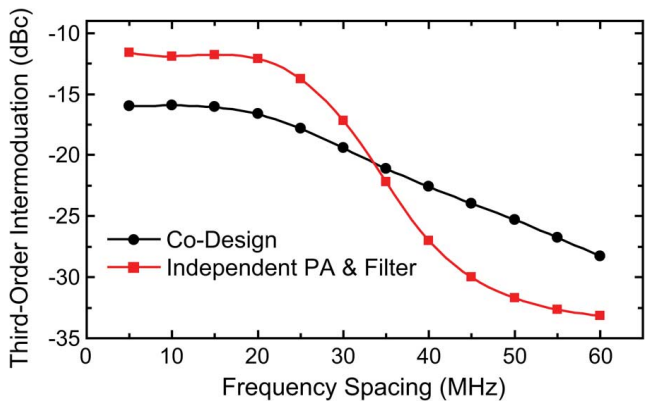

Fig. 20. Comparison of linearity performance (simulated IM3 at saturated power) between conventional and co-design modules.

design of the PA and filter building blocks in a microwave transmitter front-end.

The linearity performances of these two cases are also compared. Fig. 20 shows the simulated IM3 at saturated power level versus different frequency spacing (Δf) of the two tones. For small Δf (<20 MHz), the co-designed PA and filter exhibits lower IM3, indicating a better intrinsic linearity of the PA due to the fact that the IM3 components are still located in the passband. When Δf is larger than 20 MHz, the IM3 decreases due to the filtering effect, while the conventional design starts to present better linearity. In general, the linearity feature of the co-designed PA and filter compares favorably to the conventional design, which means that the validated efficiency enhancement is not achieved by suffering linearity.

VI. Conclusion

This paper has presented an innovative co-design method of the PA in cascade with a high-Q bandpass filter. Instead of matching the transistor to 50-Ω impedance and connecting to a 50-Ω filter, the transistor is directly integrated with the filter, thus eliminating the conventional OMN of the PA. This reduces the circuit size, complexity, and loss to the lowest possible level, eventually leading to a higher overall efficiency. As a key enabling technique, this paper develops a systematical methodology of designing the matching-filter with non-50-Ω input impedance. A two-pole EVA filter is designed and implemented as the OMN of a 10-W GaN transistor, yielding optimally tuned fundamental and harmonic impedances. A desired Chybeshev filter behavior is obtained with the co-designed PA-filter circuit module, which also presents an excellent PA performance in the passband in terms of both efficiency and linearity. Specifically, 72% efficiency, 10-W output power, >10-dB gain, and 60-dBm OIP3 were measured. These promising results demonstrate that this co-design technology achieves a global optimization in transmitter design, while it is expected to be in great demand for many applications that require a compact circuit size.

Acknowledgment

The authors would like to thank T.-C. Lee and E. Naglich, both with Purdue University, West Lafayette, IN, USA, for helpful discussions and technical assistance. The authors are also grateful to Cree Inc., Durham, NC, USA, for supplying the transistor model.

References

[1] M. Yu and Y. Wang, "Enhanced microwave multiplexing network," *IEEE Trans. Microw. Theory Techn.*, vol. 59, no. 2, pp. 270–277, Feb. 2011.

[2] C. Kudsia, R. Cameron, and W.-C. Tang, "Innovations in microwave filters and multiplexing networks for communications satellite systems," *IEEE Trans. Microw. Theory Techn.*, vol. 40, no. 6, pp. 1133–1149, Jun. 1992.

[3] R. Cameron, C. M. Kudsia, and R. R. Mansour, *Microwave Filters for Communications Systems: Fundamentals, Design, and Applications*. Hoboken, NJ, USA: Wiley, 2007.

[4] T. Hung, H. Rode, L. E. Larson, and P. M. Asbeck, "Design of H-bridge class-D power amplifiers for digital pulse modulation transmitters," *IEEE Trans. Microw. Theory Techn.*, vol. 55, no. 12, pp. 2845–2855, Dec. 2007.

[5] J. A. Weldon, R. S. Narayanaswami, J. C. Rudell, L. Lin, M. Otsuka, S. Dedieu, L. Tee, K. Tsai, C. Lee, and P. R. Gray, "A 1.75-GHz highly integrated narrowband CMOS transmitter with harmonic-rejection mixers," *IEEE J. Solid-State Circuits*, vol. 36, no. 12, pp. 2003–2015, Dec. 2001.

[6] P. Reynaert, "Polar modulation," *IEEE Microw. Mag.*, vol. 12, no. 1, pp. 46–51, Feb. 2011.

[7] D. R. Parveg, P. Singerl, A. Wiesbauer, H. M. Nemati, and C. Fager, "A broadband, efficient, overdriven class-J RF power amplifier for burst mode operation," in *Proc. 40th Eur. Microw. Conf.*, Sep. 2010, pp. 1666–1669.

[8] E. Serebryakova, A. Samulak, K. Blau, and M. Hein, "Reconstruction filters for switch-mode power amplifier systems," in *Proc. 39th Eur. Microw. Conf.*, Oct. 2009, pp. 1453–1456.

[9] C. Patel, M. Yavuz, and S. Nanda, "Femtocells," *IEEE Wireless Commun.*, vol. 17, no. 5, pp. 6–7, Oct. 2010.

[10] P. Lin, J. Zhang, Y. Chen, and Q. Zhang, "Macro-femto heterogeneous network deployment and management: From business models to technical solutions," *IEEE Wireless Commun.*, vol. 18, no. 3, pp. 64–70, Jun. 2011.

[11] S. Blasubramanian, S. Boumaiza, H. Sarbishaei, T. Quach, P. Orlando, J. Volakis, G. Creech, J. Wilson, and W. Khalil, "Ultimate transmission," *IEEE Microw. Mag.*, vol. 13, no. 1, pp. 64–82, Jan. 2012.

[12] X. Liu, L. P. B. Katehi, W. J. Chappell, and D. Peroulis, "A 3.4–6.2 GHz continuously tunable electrostatic MEMS resonator with quality factor of 460–530," in *IEEE MTT-S Int. Microw. Symp. Dig.*, Jun. 2009, pp. 1149–1152.

[13] X. Liu, L. P. B. Katehi, W. J. Chappell, and D. Peroulis, "High-Q continuously tunable electromagnetic cavity resonators and filters using SOI-based RF MEMS actuators," *IEEE/ASME J. Microelectromech. Syst.*, vol. 19, no. 4, pp. 774–784, Jul. 2010.

[14] S. Park, I. Reines, C. Patel, and G. M. Rebeiz, "High-Q RF-MEMS 4–6-GHz tunable evanescent-mode cavity filter," *IEEE Trans. Microw. Theory Techn.*, vol. 58, no. 2, pp. 381–389, Feb. 2010.

[15] H. Joshi, H. H. Sigmarsson, S. Moon, D. Peroulis, and W. J. Chappell, "High-Q fully reconfigurable tunable bandpass filter," *IEEE Trans. Microw. Theory Techn.*, vol. 57, no. 12, pp. 3525–3533, Dec. 2009.

[16] S. Moon, H. H. Sigmarsson, H. Joshi, D. Peroulis, and W. J. Chappell, "Substrate integrated evanescent-mode cavity filter with a 3.5 to 1 tuning ratio," *IEEE Microw. Wireless Compon. Lett.*, vol. 20, no. 8, pp. 450–452, Aug. 2010.
[17] E. J. Naglich, J. Lee, and D. Peroulis, "Tunable bandstop filter with a 17-to-1 upper passband," in *IEEE MTT-S Int. Microw. Symp. Dig.*, Jun. 2012, pp. 1–3.
[18] K. Chen, X. Liu, W. J. Chappell, and D. Peroulis, "Co-design of power amplifier and narrowband filter using high-Q evanescent-mode cavity resonator as the output matching network," in *IEEE MTT-S Int. Microw. Symp. Dig.*, Jun. 2011, pp. 1–4.
[19] K. Chen, X. Liu, and D. Peroulis, "Widely-tunable high-efficiency power amplifier with ultra-narrow instantaneous bandwidth," *IEEE Trans. Microw. Theory Techn.*, vol. 60, no. 12, pp. 3787–3797, Dec. 2012.
[20] G. L. Matthaei, L. Young, and E. M. T. Jones, *Microwave Filter, Impedance-Matching Networks, and Coupling Structures*. New York, NY, USA: McGraw-Hill, 1964.
[21] A. Ismail and A. Abidi, "A 3–10-GHz low-noise amplifier with wideband LC-ladder matching network," *IEEE J. Solid-State Circuits*, vol. 39, no. 12, pp. 2269–1177, Dec. 2004.
[22] M. Meng and K.-L. Wu, "Direct synthesis of general Chebyshev bandpass filters with a frequency variant complex load," in *IEEE MTT-S Int. Microw. Symp. Dig.*, May 2010, pp. 433–436.
[23] J.-S. Hong and M. J. Lancaster, *Microstrip Filters for RF/Microwave Applications*, 2nd ed. New York, NY, USA: Wiley, 2010.
[24] Advanced Design System (ADS). Agilent Technol. Inc., Santa Clara, CA, USA, 2009. [Online]. Available: http://www.agilent.com
[25] High Frequency Structure Simulator (HFSS). ver. v13.0, Ansoft Corperation, Pittsburgh, PA, USA, 2012. [Online]. Available: http://www.ansoft.com/products/hf/hfss/
[26] K. Chen, A. Semnani, and D. Peroulis, "High-power microwave gas discharge in high-Q evanescent-mode cavity resonators and its instantaneous/long-term effects," in *IEEE MTT-S Int. Microw. Symp. Dig.*, Jun. 2013, pp. 1–4.
[27] J. Moon, J. Lee, R. S. Pengelly, R. Baker, and B. Kim, "Highly efficient saturated power amplifier," *IEEE Microw. Mag.*, vol. 13, pp. 125–131, Jan. 2012.
[28] K. Chen and D. Peroulis, "Design of highly efficient broadband class-E power amplifier using synthesized low-pass matching networks," *IEEE Trans. Microw. Theory Techn.*, vol. 59, no. 12, pp. 3162–3173, Dec. 2011.
[29] K. Chen and D. Peroulis, "Design of adaptive highly efficient GaN power amplifier for octave-bandwidth application and dynamic load modulation," *IEEE Trans. Microw. Theory Techn.*, vol. 60, no. 6, pp. 1829–1839, Jun. 2012.
[30] P. Wright, J. Lees, J. Benedikt, P. J. Tasker, and S. C. Cripps, "A methodology for realizing high efficiency class-J in a linear and broadband PA," *IEEE Trans. Microw. Theory Techn.*, vol. 57, no. 12, pp. 3196–3204, Dec. 2009.
[31] J. Moon, J. Kim, and B. Kim, "Investigation of class-J power amplifier with a nonlinear $C_{\rm out}$ for optimized operation," *IEEE Trans. Microw. Theory Techn.*, vol. 58, no. 11, pp. 2800–2811, Nov. 2010.
[32] J. Kim, J. Kim, J. Moon, J. Sun, I. Kim, S. Jee, and B. Kim, "Saturated power amplifier optimized for efficiency using self-generated harmonic current and voltage," *IEEE Trans. Microw. Theory Techn.*, vol. 59, no. 8, pp. 2049–2058, Aug. 2011.
[33] P. Saad, C. Fager, H. Cao, H. Zirath, and K. Andersson, "Design of a highly efficient 2–4-GHz octave bandwidth GaN-HEMT power amplifier," *IEEE Trans. Microw. Theory Techn.*, vol. 58, no. 7, pp. 1677–1685, Jul. 2010.
[34] A. Sayed, A. A. Tanany, and G. Boeck, "5 W, 0.35–8 GHz linear power amplifier using GaN HEMT," in *Proc. 39th Eur. Microw. Conf.*, Sep. 2009, pp. 488–491.
[35] J. Kim, B. Fehri, S. Boumaiza, and J. Wood, "Power efficiency and linearity enhancement using optimized asymmetrical Doherty power amplifiers," *IEEE Trans. Microw. Theory Techn.*, vol. 59, no. 2, pp. 425–434, Feb. 2011.
[36] K. Chen and D. Peroulis, "A 3.1-GHz class-F power amplifier with 82% power-added-efficiency," *IEEE Microw. Wireless Compon. Lett.*, vol. 23, no. 8, pp. 436–438, Aug. 2013.
[37] B. Francois, P. Reynaert, A. Wiesbauer, and P. Singerl, "Analysis of burst-mode RF PA with direct filter connection," in *Proc. 40th Eur. Microw. Conf.*, Sep. 2010, pp. 974–977.

Kenle Chen (S'10) received the Bachelor's degree in communication engineering from Xi'an Jiaotong University, Xi'an, China, in 2005, the Master's degree in electronics and information engineering from Peking University, Beijing, China in 2008, and the Ph.D. degree in electrical and computer engineering from Purdue University, West Lafayette, IN, USA in 2013.

From 2007 to 2008, he was with the Institute of Micro Electronics, National Key Laboratory of Micro/Nano Fabrication, Peking University, where his research focused on RF microelectromechanical systems (MEMS) switches, tunable filters, and vacuum packaging. He is currently with the School of Electrical and Computer Engineering and Birck Nanotechnology Center, Purdue University. His research interests include broadband highly efficient PA design methodologies, adaptive PAs and transmitters, integration of PA and high-Q filters (co-design technique), and high power failure mechanisms of microwave devices.

Dr. Chen was the recipient of the 2012 IEEE Microwave Theory and Techniques Society (IEEE MTT-S) Graduate Research Fellowship. He was also the recipient of the Second and Third Place Awards of the Student High Efficiency Power Amplifier Design Competition of the IEEE MTT-S International Microwave Symposium (IMS) in 2012 and 2011, respectively.

Juseop Lee (A'02–M'03) received the B.E. and M.E. degrees in radio science and engineering from Korea University, Seoul, Korea, in 1997 and 1999, respectively, and Ph.D. degree in electrical engineering from The University of Michigan at Ann Arbor, Ann Arbor, MI, USA, in 2009.

In 1999, he joined LG Information and Communications (now LG Electronics), Seoul, Korea, where his activities included design and reliability analysis of RF components for code-division multiple-access (CDMA) cellular systems. In 2001, he joined the Electronics and Telecommunications Research Institute (ETRI), Daejeon, Korea, where he was involved in the design of passive microwave equipment for Ku- and Ka-band communications satellites. In 2005, he joined The University of Michigan at Ann Arbor, where he was a Research Assistant and Graduate Student Instructor with the Radiation Laboratory, during which time his research activities have focused on millimeter-wave radars and synthesis techniques for multiple-passband microwave filters. In 2009, he joined Purdue University, West Lafayette, IN, USA, where he was a Post-Doctoral Research Associate, during which time his activities included the design of adaptable RF systems. In 2012, he joined Korea University, Seoul, Korea, where he is currently an Assistant Professor. He is listed in *Who's Who in America*. His research interests include RF and microwave components, satellite transponders, wireless power transfer, and electromagnetic theories.

Dr. Lee was a recipient of the Freshman Award of Korea University, the Undergraduate Fellowship of Korea University, the Graduate Fellowship of LG Information and Communications, and the Graduate Fellowship of the Korea Science and Engineering Foundation. He was a recipient of the Rackham Predoctoral Fellowship of the Rackham Graduate School, The University of Michigan at Ann Arbor. He was also the recipient of the IEEE Microwave Theory and Techniques Society (IEEE MTT-S) Graduate Fellowship. He coauthored a paper that received the 2nd Place Award of the 2010 IEEE MTT-S International Microwave Symposium Student Paper Competition.

William J. Chappell (S'98–M'02–SM'10) received the B.S.E.E., M.S.E.E., and Ph.D. degrees from The University of Michigan at Ann Arbor, Ann Arbor, MI, USA, in 1998, 2000, and 2002, respectively.

He is currently an Associate Professor with the School of Electrical and Computer Engineering, Purdue University, West Lafayette, IN, USA, where he is also a member of the Birck Nanotechnology Center and the Center for Wireless Systems and Applications. His research focus is on advanced applications of RF and microwave components. He has been involved with numerous Defense Advanced Research Projects Agency (DARPA) projects involved in advanced packaging and material processing for microwave applications. His research group uses electromagnetic

analysis, unique processing of materials, and advanced design to create novel microwave components. His specific research interests are the application of very high-quality and tunable components utilizing multilayer packages. In addition, he is involved with high-power RF systems, packages, and applications. His research sponsors include HSARPA, the Office of Naval Research (ONR), the National Science Foundation (NSF), the State of Indiana, the Communications–Electronics Research, Development and Engineering Center (or CERDEC), and the Army Research Office (ARO), as well as industry sponsors.

Dr. Chappell was the IEEE Microwave Theory and Techniques Society (IEEE MTT-S) Administrative Committee (AdCom) secretary for 2009 and was elected to the IEEE MTT-S AdCom (2010–2012).

Dimitrios Peroulis (S'99–M'04) received the Ph.D. degree in electrical engineering from The University of Michigan at Ann Arbor, in 2003.

Since August 2003, he has been with Purdue University. He leads the Adaptive Radio Electronics and Sensors (ARES) team with a focus on reconfigurable analog/RF electronics for adaptive communications, signal intelligence, and harsh-environment sensors. He has been a Principle Investigator (PI)/co-PI in over 40 projects funded by government agencies and industry in these areas. Since 2007, he has been a key contributor to the Defense Advanced Research Projects Agency (DARPA) Analog Spectral Processors (ASPs) (Phases I–III) project resulting in the first widely tunable (tuning range $>$3:1) pre-select radio filters with unprecedented quality factors ($Q > 1000$) and power handling ($>$10 W) for high-frequency applications (1–30 GHz). A wide variety of reconfigurable filters with simultaneously adaptable features including frequency, bandwidth, rejection level, filter order, and group delay have been demonstrated over the past four years. His group recently co-developed a ground-breaking concept of field programmable filter arrays (FPFAs). Inspired by FPGAs in digital systems, FPFAs are based on a sea of coupled resonators and multiple ports in order to enable re-utilization of the same adaptive resonators to support diverse needs for dissimilar systems. Arbitrary operational modes and multiple operational channels may be created and reconfigured at will. Moreover, he has made significant advances in high-power high-efficient PAs and RF CMOS integrated circuits (ICs) with high-efficiency antennas. In the areas of sensors, he has demonstrated the first wireless battery-free high-temperature microelectromechanical systems (MEMS) sensors for health monitoring of sensitive bearings in aircraft engines. These sensors continuously monitor (RF identification (RFID) type) the true temperature of the bearing to over 300 °C or 550 °C (depending on the design) and wirelessly transmit it to a base station. These sensors are based on well-established silicon processing for low-cost high-yield manufacturing. They have demonstrated extremely robust operation for over 1B cycles and continuous loading for over three months without failure.

Prof. Peroulis and his team were the third place winners in the Student Power Amplifier Design Competition, 2011 IEEE Microwave Theory and Techniques Society (IEEE MTT-S) International Microwave Symposium (IMS). In addition, a student design team, for which he was assistant team leader, at Purdue University won the First Place Awards in Phases I and II of the 2007–2008 SRC/SIA IC Design Challenge by demonstrating high-efficiency chip-to-chip wireless links with U-band transceivers. Further advances led to bondwire Yagi antenna arrays with efficiencies exceeding $>$80%.